Hydroxyl and sulfate radical-based oxidation of RhB dye in UV/H2O2 and UV/persulfate systems: Kinetics, mechanisms, and comparison

Xinxin Ding, Leonardo Gutierrez, Jean-Philippe Croué, Minrui Li, Lijun Wang, Yuru Wang

Hydroxyl and sulfate radical-based oxidation of RhB dye in UV/H_2O_2 and UV/persulfate systems: kinetics, mechanisms, and comparison

Xinxin Ding [a], Leonardo Gutierrez [b], Jean-Philippe Croue [c]*,

Minrui Li [a], Lijun Wang [a], Yuru Wang [a]*

[a] Department of Environmental Science, School of Geography and Tourism, Shaanxi Normal University, Xi'an 710119, China

[b] Facultad del Mar y Medio Ambiente, Universidad del Pacifico, Ecuador

[c] Institut de Chimie des Milieux et des Matériaux IC2MP UMR 7285 CNRS, Université de Poitiers, France

*: Corresponding authors
E-mail address: jean.philippe.croue@univ-poitiers.fr; wangyuru@snnu.edu.cn

Abstract

The degradation kinetics and mechanisms of Rhodamine B (RhB) dye by $^{\bullet}OH$ and $SO_4^{\bullet-}$ based advanced oxidation processes were investigated. The $^{\bullet}OH$ and $SO_4^{\bullet-}$ radicals were generated by UV photolysis of hydrogen peroxide and persulfate (i.e., UV/H_2O_2 and UV/PS), respectively. The effects of initial solution pH, RhB concentration, oxidant dosage, Fe^{2+} concentration, and water matrices were examined. The results showed that the degradation of RhB followed pseudo-first-order kinetics in both processes, with the UV/H_2O_2 process exhibiting better performance than that of the UV/PS process. Acidic conditions were favorable to the degradation of RhB in both systems. Increasing the oxidant dosage or decreasing the contaminant concentration could enhance the degradation of RhB. Photo-Fenton-like processes accelerated the performance when Fe^{2+} was added into both systems. The removal efficiency of RhB was inhibited upon the addition of Humic Substances. The addition of Cl^- displayed no significant effect and promoted RhB degradation in UV/H_2O_2 and UV/PS systems, respectively. The presence of NO_3^- promoted RhB degradation, while $H_2PO_4^-$ and $C_2O_4^{2-}$ showed an inhibitory effect on both UV/H_2O_2 and UV/PS processes. Radical scavenging tests revealed the dominant role of $SO_4^{\bullet-}$ radicals in the UV/PS system. Furthermore, the evolution of low molecular weight organic acids and NH_4^+ during the degradation of RhB in these two processes were compared. Both UV/H_2O_2 and UV/PS systems led to similar formation trends of NH_4^+ and some ring-opening products (e.g., formic acid, acetic acid, and oxalic acid), suggesting some analogies in the decay pathways of RhB by $^{\bullet}OH$ and $SO_4^{\bullet-}$-induced oxidation processes.

Keywords: Hydroxyl radical, Sulfate radical, UV/H_2O_2, UV/PS, Rhodamine B

1. Introduction

Dyes are mainly aromatic and heterocyclic compounds with stable structures incorporating color-display and polar groups, widely used in textile, plastic, cosmetics, medicine, food, and other industries (GilPavas et al., 2019). Briefly, more than 1.28×10^6 tons of commercial dyes were produced world-wide in 2018 (Zhou et al., 2019). Remarkably, approximately 5-15% of the dyes are released into the environment during their production and dyeing processes; thus, leading to the generation of wastewater with dye concentrations varying from 5 to 1500 mg/L (Dong et al., 2010; Kim et al., 2015). These organic pollutants can disrupt photosynthesis, inhibit the growth of aquatic biota, and pose considerable health risks to human skin, eyes, gastrointestinal, and respiratory systems (Dong et al., 2010; Wang and Chu, 2011; Su et al., 2013). Consequently, dye-containing effluents discharged into the environment without proper treatment can have major negative impacts on both aquatic ecosystems and human health. Besides, dyes are generally resistant to light, aerobic digestion, and other conventional treatment processes due to their complex structures (Xu and Li, 2010; GilPavas et al., 2019; Masi et al., 2019). Therefore, the development of efficient and economical technologies for the degradation of dye contaminants from wastewater before discharge is of critical importance.

Recently, UV-based Advanced Oxidation Processes (AOPs) have drawn increasing scientific attention for degrading various types of refractory organic pollutants in water (Wang et al., 2017; Nihemaiti et al., 2018; Liu et al., 2020). Particularly, the UV/H_2O_2 process is an attractive option for the production of non-selective and highly reactive $^{\bullet}OH$ radical (E_0 = 1.8 - 2.7 V), which displays a second-order rate constant with numerous contaminants at a near diffusion-controlled

63 rate ($k=10^{10}$ $M^{-1}S^{-1}$) (Buxton et al., 1988; Keen and Linden, 2013). Besides, persulfate (PS) has
64 also emerged as an alternative oxidant due to its capacity to generate sulfate radical ($SO_4^{\bullet-}$) under
65 UV irradiation (i.e., UV/PS). $SO_4^{\bullet-}$ is a strong oxidant (E_0 = 2.5 - 3.1 V) with an oxidizing ability
66 comparable to $^{\bullet}OH$; however, showing higher selectivity and longer half-life than $^{\bullet}OH$ (Neta et al.,
67 1988; Rao et al., 2019). Compared to H_2O_2, the advantages of persulfate as a radical
68 precursor include: relative stability in solid-state, high aqueous solubility, and high stability at
69 ambient environments, which facilitate its transport, storage, and usage (Zhang et al., 2014).
70 Therefore, $SO_4^{\bullet-}$ has also been increasingly tested in the removal of bio-recalcitrant organic
71 pollutants (Zhang et al., 2013; Khan et al., 2017). Both UV/H_2O_2 and UV/PS processes have
72 demonstrated their effectiveness at degrading a wide range of organic pollutants, including
73 antibiotics, iodinated X-rays contrast media, and other PPCPs (Nihemaiti et al., 2018; Zhao et al.,
74 2019; Liu et al., 2020).

75 Rhodamine B (RhB) is a water-soluble xanthene dye mainly used as an additive in food stuffs;
76 however, it was banned in many countries due to its toxicity and carcinogenicity. The toxicity of
77 RhB has been well documented in the literature (Nestmann et al., 1979). Nevertheless, RhB is still
78 extensively applied as a colorant in textile dyeing, resulting in the production of large amounts of
79 RhB-containing effluents. Due to its high solubility and color rendering, water containing RhB,
80 even at low concentrations, can significantly impact the quality of surface water and disrupt the
81 photosynthesis of aquatic organisms (Su et al., 2013). Various UV-based AOPs have been
82 investigated for the effectiveness of RhB degradation. Zhang et al. (2020) reported that
83 approximately 90% of RhB removal was obtained in a UV enhanced electro-Fenton process where
84 $^{\bullet}OH$ radical was found as the dominant radical species. Chen et al. (2012) revealed the good

85 degradation efficiency of RhB dye in a $SO_4^{\bullet-}$-based UV/PS process and evaluated the influence of
86 some factors (e.g., oxidant dose and water matrix) on the degradation kinetics. Previous studies
87 indicated that the UV/PS process degraded organics more efficiently in buffered pure water than
88 that of the UV/H_2O_2 process, while the process performance was significantly reduced when
89 applied to wastewater effluent due to the higher sensitivity and selectivity of $SO_4^{\bullet-}$ radical toward
90 water matrix and organics compared with $^{\bullet}OH$ radical (Nihemaiti et al., 2018), suggesting the
91 significant role of water matrix and compound property on the performance of these two
92 UV-AOPs. However, to the best of our knowledge, there are no previous studies systematically
93 comparing hydroxyl and sulfate radical-based AOPs for the removal of RhB dye in water. Besides,
94 the decay pathways regarding the aromatic intermediates during the degradation of RhB by
95 hydroxyl and sulfate radical oxidation have been proposed in previous studies (He et al., 2009; Hu
96 et al., 2017; Rasheed et al., 2018). Nevertheless, limited information is available focusing on the
97 evolution of low molecular weight (LMW) carboxylic acids upon the ring-opening of aromatic
98 byproducts of RhB, which are usually more refractory towards further mineralization.

99 Therefore, the efficiency and degradation kinetics of UV/H_2O_2 and UV/PS processes to
100 degrade RhB in synthetic wastewater were investigated and compared in this study. The influence
101 of some important experimental parameters (e.g., initial solution pH, oxidant dosage, and the
102 presence of oxidant activator) and solution chemistry (e.g., inorganic ions and dissolved organic
103 matter) on the efficiency of these oxidation processes was evaluated. Radical scavenging
104 experiments were conducted to identify the dominant radical species responsible for the RhB
105 decay. Furthermore, the evolution of some LMW organic intermediates (e.g., carboxylic acids)
106 and inorganic ions produced upon the degradation of RhB was examined, and the possible

degradation mechanism was accordingly proposed. The current investigation will highly assist in better understanding the oxidation of RhB by UV/H_2O_2 and UV/PS processes for the successful implementation of these technologies in the treatment of dye-contaminated wastewaters.

2. Materials and methods

2.1. Chemical reagents

All chemical reagents were of analytical grade and used as received without further purification. Potassium persulfate ($k_2S_2O_8$, >99%), methanol (CH_3OH, 99.9%), and tert-butanol ($C_4H_{10}O$, 99%) were purchased from Sigma-Aldrich. Rhodamine B ($C_{28}H_{31}ClN_2O_3$), hydrogen peroxide (H_2O_2, 30%), nitrobenzene (NB), benzoic acid (BA), sodium thiosulfate ($Na_2S_2O_3$), potassium chloride (KCl), ferrous sulfate heptahydrate ($Fe_2SO_4 \cdot 7H_2O$), sodium oxalate ($C_2Na_2O_4$, 99.8%), potassium dihydrogen phosphate (K_2HPO_4), and sodium nitrate ($NaNO_3$) were provided by Sinopharm Chemical Reagent Co., Ltd. (China). The humic substances (hydrophobic acid fraction, i.e., DOM adsorbed onto XAD-8® resin at acid pH and recovered by caustic desorption) used in this study were previously extracted from Suwannee River water (USA). Ultrapure water (conductivity of 18.25 M Ω·cm) used in the experiments was obtained from the Cascada™ BIO water purification system (Pall Corporation, United Kingdom).

2.2. Experimental procedures

The irradiation experiments were performed in quartz tubes under continuous stirring and temperature control (20±2°C) with a photochemical reaction apparatus (BL-GHX-V, Shanghai Bilang Instrument Co., Ltd., China), equipped with a 300 W medium-pressure ultraviolet mercury lamp (λ_{max} = 365 nm) provided by the same manufacturer as the UV light source. Eight tubular quartz reactors were evenly distributed in a circle centered around the lamp with a radius of 9.5

129 cm. The schematic illustration of the experimental setup and the irradiation spectrum of the light
130 source are provided in Figs. S1 and S2 in the Supplementary Information (SI) , respectively. The
131 average UV fluence rate (Ep^0) entering the solution was determined as 2.67 mW/cm^2 by
132 iodide/iodate chemical actinometry (Bolton et al., 2011). The final applied fluence was 2060
133 mJ/cm^2, unless otherwise stated. The photochemical reactor and temperature control system were
134 turned on at least 20 min in advance to ensure stable conditions at the start of the experiments.

135 The degradation kinetics of RhB in the UV/H_2O_2 or UV/PS process were investigated by
136 sequentially spiking a specific amount of RhB, H_2O_2, or PS stock solution in ultrapure water. The
137 initial pH of the solution was adjusted with sulfuric acid (0.1 M) and sodium hydroxide (0.1 M).
138 No buffer solution was used in this study to avoid potential reactions between the radicals and
139 buffer solution. The reaction was initiated by adding a specific amount of H_2O_2 or PS into the
140 aqueous solution containing the probe contaminant while simultaneously subjected to UV
141 irradiation. The reaction volume of the solutions was set at 50 mL. The samples were collected at
142 predetermined time intervals and immediately quenched by adding sodium thiosulfate in excess.
143 There is some uncertainty in the literature regarding the effectiveness of sulfur-based reductants
144 (e.g., bisulfite and thiosulfate) as a quencher of H_2O_2 as reported by Wang et al. (2019).
145 Nevertheless, preliminary experiments conducted at pH from 2 to 11 demonstrated the
146 insignificance of H_2O_2 or PS alone for the RhB degradation (Fig. S3). Thus, the potential effect of
147 any residual oxidant on the decay result of RhB should be negligible. The collected samples were
148 filtered through a 0.45 μm membrane before analysis with High-Performance Liquid
149 Chromatography (HPLC).

150 *2.3. Analytical methods*

151 The residual concentrations of RhB, NB, and BA were determined using a Dianex UltiMate
152 3000 HPLC system measuring the absorbance at 554, 270, and 230 nm, respectively. The
153 separation was performed on a Pinnacle II C18 column (250 mm × 4.6 mm with i.d. of 5 μm,
154 Restek). The mobile phase consisted of 60% acetonitrile and 40% water (V/V), while the flow rate
155 was set at 1.0 mL/min. The separation of LMW organic acids and ammonia was conducted by a
156 Dionex IC-1500 Ion Chromatography interfaced with a Dionex DS6 Conductivity Detector. A
157 Dionex IonPac AS19 column (4 mm × 250 mm) with its respective guard column (IonPac AG19,
158 4 mm ×50 mm) was used for the separation of LMW organic acids with a KOH gradient elution
159 (conditioning: 5 min at 1 mM; elution: 28 min at 18 mM to 35 mM, rinsing: 5 min at 1 mM) at a
160 flow rate of 1.0 mL/min. For ammonia analysis, a Dionex IonPac CG12A guard column (4 mm ×
161 50 mm) connected to an IonPac CS12A analytical column (4 mm × 250 mm) was used; while
162 eluted by 20 mM methanesulfonic acid at a flow rate of 1.0 mL/min. The Total Organic Carbon
163 (TOC) content of the samples was determined using a TOC-LCPH analyzer (Shimadzu, Japan)
164 through catalytic combustion oxidation at 680℃ and analysis with a non-dispersive infrared
165 detector.

166 ## 3. Results and discussion

167 ### *3.1. RhB degradation kinetics in different oxidation systems*

168 The degradation of RhB in different oxidation systems including H_2O_2 alone, PS alone, UV
169 irradiation, UV/H_2O_2, and UV/PS at neutral solution pH was investigated and compared. The
170 degradation of RhB by H_2O_2 or PS alone was negligible, indicating that in the absence of
171 activation these two oxidants are ineffective toward RhB at neutral pH (Fig.1). Under
172 UV irradiation, the removal of RhB reached 45% after 6 minutes of exposure. An enhanced

degradation was observed when UV irradiation was conducted in the presence of H_2O_2 or PS due to the expected generation of $^{\bullet}OH$ and/or $SO_4^{\bullet-}$ radicals. Remarkably, UV/H_2O_2 was more efficient than UV/PS for the removal of RhB. Only 2 minutes and 4 minutes of irradiation were necessary to decrease the concentration of RhB by 50% for UV/H_2O_2 and UV/PS process, respectively (Fig. 1a). After 15 min, approximately 96% and 87% of RhB were removed by the UV/H_2O_2 and UV/PS processes, respectively. The reactions followed pseudo-first-order kinetics (R^2>0.97) (Fig. 1b) The experimental rate constants (k_{obs}) derived from the slope of ln(C/C_0) versus time were 0.080, 0.150, and 0.219 min^{-1} for UV, UV/PS, and UV/H_2O_2, respectively.

3.2. Effect of initial solution pH on the degradation kinetics

The influence of initial solution pH ranging from 2 to 11 on RhB degradation in UV/H_2O_2 and UV/PS systems was investigated (Fig. S4, SI). For all pH conditions, the reaction in the two systems followed pseudo-first-order kinetics (R^2>0.98). The decay rate constant (k_{obs}) of RhB in both UV-based AOP systems significantly decreased with increasing pH (i.e., from pH 2 to 7); however, k_{obs} remained approximately constant from pH 7 to 11 (Fig. 2).

This general pH trend on the degradation of RhB by AOPs was previously observed by others, i.e., UV/H_2O_2 (Daneshvar et al., 2008), UV/$S_2O_8^{2-}$ (Chen et al., 2012), Ozone/H_2O_2 (Bai et al., 2011). The decrease in the process efficiency with increasing pH was also demonstrated for other molecules e.g., ofloxacin, levofloxacin, and thiamphenicol with UV/H_2O_2 or UV/PS (Wang et al., 2017; Liu et al., 2020). All these studies attributed this result, to a large extent, to the higher production of radicals under acidic pH conditions and the scavenging and competing reactions occurring at more alkaline pH. The role of hydroxyl ions in the complex propagation and termination radical reaction mechanisms influencing the stability and reactivity of the produced

radical species have been well described in the above-listed publications and review articles (Stefan, 2017). The competing reactions with the formed by-products and the radical scavenging effect of carbonate species (bicarbonate and carbonate ions) at neutral and alkaline pHs produced from the degradation of the target compound (Criquet and Leitner, 2009) or possibly introduced from enhanced dissolution from atmospheric CO_2 are also of significant importance (Baeza and Knappe, 2011). The impact of carbonate species on the performance of UV/H_2O_2 and UV/PS treatment processes for contaminant degradation has been well documented (Wang et al., 2017; Nihemaiti et al., 2018).

It is also accepted that the change in molar absorptivity and quantum yield with the pH of the targeted compound can have a significant impact on the pseudo-first-order rate constant (Shen and Lin, 2003). Baeza and Knappe (2011) have noted that the impact of the pH on the UV/H_2O_2 AOP efficiency varied depending on the presence of either the neutral or the charged form (anionic or cationic) of the molecule (i.e., as a function of pK_a), which significantly influenced the direct photolysis rate constant but had little effect on the hydroxyl radical oxidation rate. RhB is characterized by a pK_a value of 3.1 (Arbeloa and Ojeda, 1982) or 3.7 (Wang et al., 2014). Increasing the pH from 2 to 4 implies a change in the molecular conformation of RhB from its cationic form to its neutral/zwitterion form, a change that can possibly influence the degradation efficiency of both AOPs. The direct photolysis rate of RhB (k = 0.080 min^{-1} at pH 7), which contributes to a large part of the degradation of the molecule, should not differ above pH 4. No significant change of the k_{obs} was noted from pH 7 to 11, which suggests a relatively constant contribution of the radical species to the degradation of RhB.

Results depicted in Fig.2 showed similar k_{obs} of RhB for the two AOPs at acid pH (pH<7) and high alkaline pH (pH 11). This similarity was not observed in the previous referred studies. At acid pH, $^{\bullet}OH$ and $SO_4^{\bullet-}$ radicals are predominant in the UV/H_2O_2 and UV/PS treatment processes, respectively. At very high pH 11, the reaction between $SO_4^{\bullet-}$ and OH^- becomes significant, converting most of $SO_4^{\bullet-}$ radicals to $^{\bullet}OH$ radicals (Fang et al., 2012). At pH 11, the RhB solution was subjected to $^{\bullet}OH$ radical attack only in both AOP conditions. At a solution pH ranging from 7 to 9, $SO_4^{\bullet-}$ and $^{\bullet}OH$ radicals were simultaneously present in the system; for this pH condition the pseudo-first-order rate constant determined under UV/H_2O_2 treatment was systematically higher than the one obtained for the UV/PS process. The nature and/or the relative abundance of the formed by-products in this pH range may differ from the two AOPs and control the degradation rate of RhB.

3.3. Effect of the initial RhB concentration and oxidant dose

The degradation efficiency of RhB at pH 7 decreased with increasing initial RhB concentration in both UV/H_2O_2 and UV/PS systems after 15 min reaction time (Fig.3a). At concentrations of 2.5, 5, 10, and 20 μM, the degradation efficiencies in the UV/H_2O_2 system were 98.8%, 98.7%, 95.6%, and 65.3%; and 100%, 98.3%, 86.7%, and 59.0% in the UV/PS system, respectively. In the UV/H_2O_2 system, the pseudo-first-order reaction constant k_{obs} (R^2 >0.98) gradually decreased from 0.555 to 0.106 min^{-1} as the RhB concentration increased from 2.5 to 20 μM; while in the UV/PS system, the k_{obs} decreased from 0.841 to 0.085 min^{-1}, respectively. The decrease of k_{obs} with increasing RhB concentration can be explained as follows.

Firstly, RhB exhibits two main absorption peaks at 259 nm and 554 nm. The absorption of RhB at the UV region can hinder the efficiency of the UV-based AOPs by reducing the amount of

applied fluence. In this study, an increase in RhB concentration from 2.5 to 20 μM led to an increase of UV absorbance at 254 and 365 nm from 0.165 to 0.497 and 0.066 to 0.163, respectively, which significantly enhanced its inner filter effect and resulted in a decrease in the corresponding applied fluence by 38.9% and 15.1%, respectively. Consequently, the available UV fluence for activating H_2O_2 and PS for $^{\bullet}OH$ and $SO_4^{\bullet-}$ production was remarkably reduced; thus, decreasing the amount of $^{\bullet}OH$ and/or $SO_4^{\bullet-}$ available to react with the target compound. Secondly, the byproducts generated in solution at high RhB dose also compete with their mother compound for $^{\bullet}OH$ and $SO_4^{\bullet-}$ consumption and in turn decrease the overall RhB decay (Wang and Chu, 2011). These results are consistent with previous observations by Rehman et al. (2018) and Isari et al. (2018), indicating that the initial concentration of the contaminant is an important factor affecting its degradation rate.

As the precursor of active radicals, the concentrations of H_2O_2 and PS play a decisive role in the overall degradation efficiency of the UV/H_2O_2 and UV/PS processes (Fig. S5, SI). Experimental results showed that increasing the H_2O_2 concentration from 10 to 200 μM, led to a considerable enhancement in the removal of RhB in the UV/H_2O_2 system (i.e., from 63% to almost 99% after 10 min treatment), resulting in a significant increase in the corresponding decay rate constant (i.e., from 0.101 to 0.408 min^{-1} in Fig. 3b). Similar results were obtained with the UV/PS system. However, a large excess of H_2O_2 might induce enhanced scavenging effect by reacting with $^{\bullet}OH$ to produce less reactive species (conditions not studied in the current research), which in turn would decrease the degradation rate of the target contaminant (Eqs. 1 and 2) (Christensen et al., 1982; Pouran et al., 2015; Wang et al., 2017; Tian et al., 2019). Similarly, an over-dosage of PS in the system can also inhibit the process efficiency because the side reactions

between PS and the generated $SO_4^{\bullet-}$/$^{\bullet}OH$ radicals to generate $S_2O_8^{\bullet-}$ (Eqs. 3 and 4) become more substantial, while $S_2O_8^{\bullet-}$ is less reactive than $SO_4^{\bullet-}$; thus, inducing a quenching effect (Liang and Su, 2009).

$$H_2O_2 + {}^{\bullet}OH \rightarrow HO_2^{\bullet} + H_2O \qquad k = 2.7\times10^7\ M^{-1}S^{-1} \qquad (1)$$

$$HO_2^{\bullet} + {}^{\bullet}OH \rightarrow O_2 + H_2O \qquad k = 6.6\times10^9\ M^{-1}S^{-1} \qquad (2)$$

$$SO_4^{\bullet-} + S_2O_8^{2-} \rightarrow S_2O_8^{\bullet-} + SO_4^{2-} \qquad k = 6.1\times10^5\ M^{-1}S^{-1} \qquad (3)$$

$$^{\bullet}OH + S_2O_8^{2-} \rightarrow S_2O_8^{\bullet-} + OH^- \qquad k = 1.2\times10^7\ M^{-1}S^{-1} \qquad (4)$$

3.4. The multi-role of Fe^{2+} as an oxidant activator

The influence of Fe^{2+} as a transition metal activator of H_2O_2 and PS on the degradation of RhB in H_2O_2, PS, UV/H_2O_2, and UV/PS systems was investigated (Fig. S6, SI). The initial solution pH was adjusted as 3 to avoid the oxidation of Fe^{2+} into Fe^{3+} and its subsequent precipitation. The calculated k_{obs} increased with increasing Fe^{2+} concentration for all conditions studied (Fig. 4). The addition of 100 μM Fe^{2+} as the activator of H_2O_2 (i.e., Fenton reagent) and PS (i.e., Fenton-like reagent), increased the k_{obs} from 0 to 0.215 min^{-1} and 0.072 min^{-1}, respectively. The efficiency of Fenton and Fenton-like reagents for the degradation of organic contaminants has been previously well described in the literature (Chamarro et al., 2001; Xu and Li, 2010).

In the UV/H_2O_2 system, the addition of 100 μM Fe^{2+} (i.e., causing the formation of a photo-Fenton system) led to an increase in the removal of RhB from 78.1% to 99.4% in 3 min; whereby the decay rate constant significantly increased by 4-fold (i.e., from 0.421 to 1.699 min^{-1}). Compared to the UV/H_2O_2 process, the substantial improvement in the process efficiency as a result of the formation photo-Fenton system can be attributed to the additional production of $^{\bullet}OH$ radicals in two ways. One way involves the favorable $^{\bullet}OH$ radical generation by the Fe^{2+}-activated

decomposition of H_2O_2 (Eq. 5). Another way providing an additional formation of $^{\bullet}OH$ radicals is due to the photoreduction of hydroxylated Fe^{3+} ions or ferrihydroxalate ($Fe(OH)^{2+}$) (Eq. 6), which can simultaneously regenerate Fe^{2+} ions and in turn further promote the process performance (Pouran et al., 2015). For the UV/PS system, when the concentration of Fe^{2+} in solution was increased to 100 μM, the target pollutant was almost completely degraded (>99%) within 3 min, while the RhB removal in the UV/PS process without Fe^{2+} ions was only 71%. Accordingly, the decay rate constant k_{obs} significantly increased from 0.366 to 1.617 min^{-1} as dosing Fe^{2+} ions from 0 to 100 μM into the system. This result indicated that the addition of Fe^{2+} to the UV/PS system remarkably enhanced the degradation efficiency of contaminants by developing a Photo-Fenton-like oxidation system. Briefly, Fe^{2+} reacted with $S_2O_8^{2-}$ to produce more $SO_4^{\bullet-}$ in the UV/PS system (Eq. 7) (Liang et al., 2008). Subsequently, the formed Fe^{3+} ions led to the generation of $Fe(OH)^{2+}$ which further photolyzed into $^{\bullet}OH$ radicals and Fe^{2+} ions; thus, accelerating the degradation of RhB (Liang et al., 2008). Compared to the traditional Fenton reaction or the UV activated H_2O_2 or PS system, the Photo-Fenton-like oxidation system could significantly improve the degradation efficiency of pollutants.

$$Fe^{2+} + H_2O_2 + h\nu \rightarrow Fe^{3+} + {}^{\bullet}OH + HO^- \quad (5)$$

$$Fe(OH)^{2+} + h\nu \rightarrow Fe^{2+} + {}^{\bullet}OH \qquad \lambda < 580\ nm \quad (6)$$

$$Fe^{2+} + S_2O_8^{2-} \rightarrow SO_4^{2-} + Fe^{3+} + SO_4^{\bullet-} \qquad k = 2.0\times10^1\ M^{-1}S^{-1} \quad (7)$$

3.5. Effect of the water matrix on the degradation of RhB

Cl^-, $H_2PO_4^-$, NO_3^-, and $C_2O_4^{2-}$ are ubiquitously present in natural water and wastewaters. They can exert varying influence on the UV-based AOPs by either acting as a radical scavenger or

297 inducing photochemical effect. Thus, the RhB degradation in the presence of Cl^-, $H_2PO_4^-$, $C_2O_4^{2-}$,
298 or NO_3^- in both UV/H_2O_2 and UV/PS systems was investigated and compared (Fig. 5a-c). The
299 concentration of chloride in natural water systems varies from around 1 to several mM. In some
300 surface waters, it may reach > 20 mM (Magazinovic et al., 2004). Accordingly, 10 mM chloride
301 was selected to investigate the effect of chloride on the process performance, while the impact of
302 other ions was conducted under the same conditions for comparison. The addition of
303 Cl^- exerted negligible impact on the UV/H_2O_2 system, as predicted from by Eqs. 8 and 9 (Atinault
304 et al., 2008). There were some $ClHO^{\bullet-}$ formed by the reaction of Cl^- and $^{\bullet}OH$; however,
305 subsequently transformed back to $^{\bullet}OH$. Thus, the whole system was relatively stable. The addition
306 of Cl^- slightly accelerated the oxidation of RhB in the UV/PS system. A similar observation was
307 reported by Huang et al. (2017), who showed that above 5 mM, chloride ions improved the
308 degradation of RhB in a sulfate radical-based oxidation system. Nevertheless, an inhibitory effect
309 at a lower chloride dosage of 0-5 mM was observed. Generally, the presence of chloride ions
310 induces dual impact depending on the Cl^- concentration and the type of substrate. A low level, Cl^-
311 mainly leads to a scavenging effect by reacting with $SO_4^{\bullet-}$ to form less reactive chlorine radicals
312 (e.g., $Cl^{\bullet}$). Interestingly, the enhanced formation of reactive chlorine species (e.g., $Cl_2^{\bullet-}$ and HClO)
313 at higher chloride dosage can compensate the consumption of $SO_4^{\bullet-}$ and even increase the process
314 efficiency. When $H_2PO_4^-$ and $C_2O_4^{2-}$ were introduced into the solution, the degradation of RhB
315 was negatively affected in both systems. This observation could be attributed to the formation of
316 $^{\bullet}H_2PO_4$ and $^{\bullet}C_2O_4^-$, which showed a relatively weak reactivity towards contaminants and a certain
317 quenching effect on $^{\bullet}OH$ and $SO_4^{\bullet-}$ radicals (Grgic et al., 2007; Xu and Li, 2010). Specifically, the
318 reactivity of $^{\bullet}OH$ and $SO_4^{\bullet-}$ with $H_2PO_4^-$ was 2.0×10^4 and 7.2×10^4 $M^{-1}s^{-1}$, respectively, while their

respective reaction rate constants with $C_2O_4^{2-}$ were (5.3±0.3)×10^6 and (1.3±0.1)×10^7 $M^{-1}s^{-1}$ (Getoff et al., 1971; Neta et al., 1988; Grgic et al., 2007; Grebel et al., 2010). Thus, the performance of both UV/H_2O_2 and UV/PS systems was significantly reduced by the addition of $C_2O_4^-$ ions compared to that of $H_2PO_4^-$ ions. Meanwhile, $C_2O_4^-$ exhibited a stronger inhibition for the UV/PS process than that of the UV/H_2O_2 process due to its higher reactivity towards sulfate radicals. RhB removal efficiency was substantially increased in the presence of NO_3^- ions and the observed rate constant of RhB decay in the UV/H_2O_2 and UV/PS systems was 1.6 and 2.2-fold of that control tests (Fig. 5c), respectively. This significant performance enhancement resulted from the formation of additional reactive species via the NO_3^- photolysis (Eqs. 10-12). The main pathway of UV irradiation of NO_3^- ions yields hydroxyl radicals which benefit the process efficiency for the UV-based AOPs (Shankar et al., 2007; Boucheloukh et al., 2012). Other studies have also reported the promoting effect of NO_3^- ions on the UV-based systems (Rao et al., 2016). However, NO_2^- formation by UV irradiation of NO_3^- might be of concern for nitrate-rich waters in the present of DOM (Semitsoglou-Tsiapou et al., 2016).

$$Cl^- + {}^{\bullet}OH \rightarrow ClHO^{\bullet-} \qquad k = 4.3\times10^9\ M^{-1}S^{-1} \qquad (8)$$

$$ClHO^{\bullet-} \rightarrow Cl^- + {}^{\bullet}OH \qquad k = 6.1\times10^9\ M^{-1}S^{-1} \qquad (9)$$

$$NO_3^- + hv \rightarrow [NO_3^-]^* \rightarrow OONO^- \qquad (10)$$

$$[NO_3^-]^* \rightarrow NO_2^- + O\ (^3p) \qquad (11)$$

$$[NO_3^-]^* \rightarrow NO_2^{\bullet} + O^{\bullet-} \xrightarrow{H_2O} NO_2^{\bullet} + {}^{\bullet}OH + OH^- \qquad (12)$$

Dissolved Organic Matter (DOM), such as Humic Substances (HS), is known to affect the behavior of organic pollutants in the environment and engineering processes. It can induce a significant influence on the performance of UV-based AOPs process by playing multiple roles.

The presence of highly reactive aromatic moieties within the DOM decreases the effective UV fluence by acting as UV inner filter and consuming radical species (e.g., the rate constants of $k_{^{\bullet}OH/NOM}$ and $k_{SO4^{\bullet-}/NOM}$ are 2.23×10^{8} and 6.0×10^{6} $M^{-1}s^{-1}$, respectively) (Westerhoff et al., 2007; Zhang et al., 2019); thus, ultimately inhibiting the degradation of contaminants. Therefore, RhB degradation in UV/H_2O_2 and UV/PS systems was investigated in the presence of the hydrophobic acid fraction isolated from the Suwannee River (HPOA-SWR). Fig. 5d illustrates the pseudo-first-order kinetics of the reaction. The presence of HPOA-SWR significantly decreased the k_{obs} of RhB decay in the two systems, displaying an exponential decrease in k_{obs} with increasing HPOA-SWR concentration. Specifically, when the concentration of DOM increased from 0 to 10 mg-C/L, the k_{obs} decreased by ~73% in both systems, and the removal of RhB decreased from 95.6% to 54% and from 86.7% to 46% in UV/H_2O_2 and UV/PS systems, respectively. The current experimental results demonstrated that the inhibitory effect of background DOM in the water matrix should be of special concern for the UV-based AOPs.

3.6. Predominant radicals in the oxidation systems

As common free radical scavengers, methanol (MeOH) can react with both $^{\bullet}OH$ and $SO_4^{\bullet-}$ radicals at high rate constants ($k_{^{\bullet}OH/MeOH}$ = 9.7×10^{8} $M^{-1}s^{-1}$ and $k_{SO4^{\bullet-}/MeOH}$ = 1.1×10^{7} $M^{-1}s^{-1}$) (Buxton et al., 1988; Neta et al., 1988); thus, effectively quenching these two radicals. Tert-butyl alcohol (TBA) exhibited a higher reaction rate with $^{\bullet}OH$ ($k_{^{\bullet}OH/TBA}$ = $(3.8\text{-}7.6)\times10^{8}$ $M^{-1}S^{-1}$), which was considerably higher than that with $SO_4^{\bullet-}$ ($k_{SO4^{\bullet-}/TBA}$ = $(4.0\text{-}9.1)\times10^{5}$ $M^{-1}S^{-1}$) (Anipsitakis and Dionysiou, 2004). Consequently, for processes involving the contribution of both $^{\bullet}OH$ and $SO_4^{\bullet-}$ radicals, TBA could selectively capture $^{\bullet}OH$ to inhibit the oxidation reaction and thereby the

specific role of •OH and $SO_4^{\bullet-}$ can be distinguished based on the different decay efficiencies. In the UV/PS process, two main reactive radicals were generated: $SO_4^{\bullet-}$ and •OH, both participating in the reaction. To identify the predominant radicals in the UV/PS system, MeOH was separately added to the solution at a ratio of 3000:1 and 1000:1 to oxidants, respectively. A similar approach was conducted for TBA. Fig. 6 illustrates the comparative decay of the target contaminant with and without radical scavengers in UV/H_2O_2 and UV/PS systems.

Experimental results showed that both TBA and MeOH were effective •OH scavengers. However, MeOH exhibited a higher scavenging capacity of radicals than TBA; thus, playing a more important role in the inhibition of RhB decay. The degradation of RhB in the UV/H_2O_2 process–significantly decreased from 96% to 17% and 46% after adding 50 mM MeOH and TBA (Fig. 6a), respectively. Increasing the concentration of TBA to 150 mM further reduced the process efficiency by approximately 10%, while the addition of 150 mM MeOH led to insignificant decrease in the RhB removal compared with that of 50 mM MeOH, suggesting that •OH radicals generated in the UV/H_2O_2 process were almost completely quenched by 50 mM MeOH. Radical scavenging experiments in the UV/H_2O_2 process indicated that •OH radicals contributed to almost 82% of RhB decay. In the UV/PS process, the addition of 50 mM MeOH and TBA inhibited the process efficiency by 78% and 35.6%, respectively (Fig. 6b). The remarkable difference between these two quenchers in the inhibitory effect on the RhB removal suggested that both $SO_4^{\bullet-}$ and •OH radicals were involved in the degradation of RhB. Moreover, the considerably more pronounced inhibition upon the addition of MeOH indicated the predominant role of $SO_4^{\bullet-}$ radicals in the UV/PS process. When the molar ratio of MeOH or TBA to PS increased from 1000:1 to 3000:1, the change in the removal of RhB was negligible.

This result confirmed that the system had relatively lower production of $^{\bullet}OH$ and the low concentration of quencher was sufficient. Based on the quenching experimental results, the contribution of $SO_4^{\bullet-}$, $^{\bullet}OH$, and direct photolysis to the degradation of RhB in the UV/PS process was determined as 40%, 31%, and 16%, respectively. Moreover, this comparison found that the two quenchers displayed a stronger inhibitory impact on the UV/H_2O_2 system, indicating a higher yield of $^{\bullet}OH$ in this system.

To further investigate the production of reactive species in UV/H_2O_2 and UV/PS systems, NB and BA were used as radical probes. NB could selectively react with $^{\bullet}OH$ following a second order rate constant of 3.9×10^9 $M^{-1}S^{-1}$, while BA reacts with both $^{\bullet}OH$ and $SO_4^{\bullet-}$ with second order rate constants of 5.9×10^9 and 1.2×10^9 $M^{-1}S^{-1}$, respectively (Guan et al., 2011). The detailed calculation of $^{\bullet}OH$ and $SO_4^{\bullet-}$ can be found in Text S1. The degradation of NB and BA in the tests followed pseudo-first-order kinetics (R^2 >0.99) (Fig. 6c and 6d). Hence, the steady-state concentration of $^{\bullet}OH$ was calculated as 4.04×10^{-13} and 2.73×10^{-13} M in UV/H_2O_2 and UV/PS systems, respectively. The concentration of $SO_4^{\bullet-}$ in the UV/PS system was 7.34×10^{-13} M. These results confirmed the predominant roles of $^{\bullet}OH$ and $SO_4^{\bullet-}$ in UV/H_2O_2 and UV/PS processes, respectively.

3.7. Intermediate identification and plausible mechanisms

To explore the mechanism of RhB degradation in the UV/H_2O_2 and UV/PS processes, the initial concentration of oxidants and RhB was increased to a relatively higher concentration of 1 mM and 0.2 mM, respectively. Simultaneously, the TOC removal and the production of some RhB decomposition intermediates (e.g., low molecular weight organic acids) were recorded by TOC analyzer and IC (Fig. 7). After 4 h of treatment, the degradation efficiencies of the RhB in

both UV/H_2O_2 and UV/PS processes were almost 100% and the TOC removal was 50% and 60%, respectively. During the degradation/decolorization of the RhB in both processes, a rapid depletion in the two characteristic absorbance peaks (i.e., 259 nm at UV region and 554 nm at the visible light region) of the RhB was observed (spectra shown in Fig. S7, SI), which corresponded to the destruction of aromatic and the chromophore structures (i.e., C=N and C=O groups) (Jiang et al., 2018), respectively. Meanwhile, five degradation intermediates were identified including one inorganic ion (i.e., NH_4^+) and four LMW organic acids, i.e., formate ($HCOO^-$), acetate (CH_3COO^-), oxalate ($C_2O_4^{2-}$), and lactate ($C_3H_5O_3^-$). These small organic acids generally resulted from the subsequent oxidation of longer-chain carboxylic acids, such as maleic and fumaric acids, upon the benzene ring opening. Therefore, the degradation of RhB could be attributed to the destruction of the conjugated groups and the N-de-ethylation upon attack by reactive radical species like $SO_4^{\bullet-}$ and $^{\bullet}OH$, causing the generation of some carboxylic acids by opening the benzene rings, where the organic nitrogen could be oxidized to form NH_4^+ after the N-position de-ethylation in the molecules.

A first formation and then decay curve was observed for lactic acid (i.e., $C_3H_5O_3^-$) in both UV/H_2O_2 and UV/PS processes. The generation of $C_3H_5O_3^-$ rapidly reached a maximum of 40.6 μM at 5 min in the UV/PS system, and then decreased. However, the yield of $C_3H_5O_3^-$ in the UV/H_2O_2 process was significantly lower with a peak concentration of 11.7 μM after 2 h. The amount of all other small carboxylic acids showed an increasing formation trend as a function of reaction time in both processes. Specifically, $C_3H_5O_3^-$ was one of the intermediates formed before RhB was mineralized into $HCOO^-$ and CH_3COO^- (smaller molecular weight). The subsequent decomposition of these intermediates upon further attack by radicals lead to a significant

accumulation of $HCOO^-$ and CH_3COO^- in both UV/H_2O_2 and UV/PS processes (Fig. 7). By comparison, the yield of $HCOO^-$ and CH_3COO^- in the UV/PS system was approximately 1.5-fold higher than that in the UV/H_2O_2 system. Meanwhile, a gradual accumulation of NH_4^+ ions was recorded in both systems due to the oxidation of the N-de-ethylation. As subsequent oxidation took place, NH_4^+ ions can be further converted into NO_3^- ions which were not detected in the current study. The buildup of NH_4^+ ions after 4 h reached 26.3 and 52.8 μM in UV/H_2O_2 and UV/PS processes, respectively. The relatively higher transformation efficiency and more production of end products in the UV/PS process indicated that at higher concentrations of both contaminants and oxidants, the UV/PS process displayed a better performance and oxidability for the RhB transformation.

4. Conclusions

In this study, UV light was used to activate H_2O_2 and PS to degrade the RhB dye in aqueous solution through the formation of $^{\bullet}OH$ and $SO_4^{\bullet-}$ radicals; whereby, the removal efficiency of RhB in the two systems and under different conditions were compared. The results showed that:

(1) Both UV/H_2O_2 and UV/PS processes displayed a good performance on the degradation of RhB, and the decay followed pseudo-first-order kinetics. The removal of RhB decreased with increasing pH, where the optimum pH value was 2 in both systems. In a certain range, the degradation efficiency increased with increasing oxidant concentration and decreasing initial concentration of RhB. The formation of photo-Fenton and photo-Fenton-like systems by adding Fe^{2+} facilitated the oxidation performance. HS remarkably suppressed the process efficiency by acting as UV inner filter and radical sink. The addition of Cl^- had no significant impact on the UV/H_2O_2 process; however, it slightly promoted the degradation in

446 the UV/PS system. The presence of NO_3^- substantially facilitated the oxidation of RhB in both
447 processes, while $H_2PO_4^-$ and $C_2O_4^{2-}$ showed the opposite effect.

448 (2) Suppression tests by adding MeOH and TBA as radical scavengers and competition
449 kinetic tests by using NB and BA as relevant radical probes confirmed the dominant role of $SO_4^{\bullet-}$
450 radicals in the UV/PS process. The steady-state concentration of $^{\bullet}OH$ was calculated as 4.04×10^{-13}
451 and 2.73×10^{-13} M in UV/H_2O_2 and UV/PS systems, respectively, while the yield of $SO_4^{\bullet-}$ in the
452 UV/PS system was 7.34×10^{-13} M in the presence of 1 μM radical probes, 10 μM RhB, and 50 μM
453 oxidants at pH 7 in aqueous solution.

454 (3) The UV/PS process led to a relative higher TOC removal compared to that of the
455 UV/H_2O_2 process in the current study. The transformation of RhB gave rise to the accumulation
456 of LMW carboxylic acids (e.g., formic acid, acetic acid, and oxalic acid) and the formation of
457 inorganic ions (i.e., NH_4^+). Accordingly, the degradation of RhB could be attributed to the opening
458 of the benzene rings and the oxidation of the organic nitrogen upon attack by $SO_4^{\bullet-}$ and $^{\bullet}OH$
459 radical species, resulting in the generation of LMW carboxylic acids and NH_4^+ as transformation
460 products.

461 **Acknowledgments**

462 The research reported in this work was supported by the National Natural Science Foundation
463 of China (No.51508317), the Fundamental Research Funds for the Central Universities
464 (GK201802108), China Postdoctoral Science Foundation (No.2016M602762), and the Special
465 Financial Grant from the Shaanxi Postdoctoral Science Foundation (No.2017BSHTDZZ09).
466

References

Anipsitakis, G.P., Dionysiou, D.D., 2004. Radical generation by the interaction of transition metals with common oxidants. Environ. Sci. Technol. 38, 3705-3712.

Arbeloa, I.L., Ojeda, P.R., 1982. Dimer states of Rhodamine B. Chem. Phys. Lett. 87, 556-560.

Atinault, E., De Waele, V., Schmidhammer, U., Fattahi, M., Mostafavi, M., 2008. Scavenging of e_s^- and OH· radicals in concentrated HCl and NaCl aqueous solutions. Chem. Phys. Lett. 460, 461-465.

Baeza, C., Knappe, D.R.U., 2011. Transformation kinetics of biochemically active compounds in low-pressure UV Photolysis and UV/H2O2 advanced oxidation processes. Water Res. 45, 4531-4543.

Bai, C.P., Xiong, X.F., Gong, W.Q., Feng, D.X., Xian, M., Ge, Z.X., Xu, N., 2011. Removal of rhodamine B by ozone-based advanced oxidation process. Desalination 278, 84-90.

Bolton, J.R., Stefan, M.I., Shaw, P.-S., Lykke, K.R., 2011. Determination of the quantum yields of the potassium ferrioxalate and potassium iodide-iodate actinometers and a method for the calibration of radiometer detectors. J. Photoch. Photobio. A 222, 166-169.

Boucheloukh, H., Sehili, T., Kouachi, N., Djebbar, K., 2012. Kinetic and analytical study of the photo-induced degradation of monuron by nitrates and nitrites under irradiation or in the dark. Photoch. Photobio. Sci. 11, 1339-1345.

Buxton, G.V., Clive L, G., W, P.H., Alberta B, R., 1988. Critical Review of rate constants for reactions of hydrated electrons, hydrogen atoms and hydroxyl radicals (·OH/·O^- in Aqueous Solution. J. Phys. Chem. Ref. Data 17, 513-886.

Chamarro, E., Marco, A., Esplugas, S., 2001. Use of Fenton reagent to improve organic chemical biodegradability. Water Res. 35, 1047-1051.

Chen, X., Xue, Z., Yao, Y., Wang, W., Zhu, F., Hong, C., 2012. Oxidation Degradation of Rhodamine B in Aqueous by UV/S2O82- Treatment System. International Journal of Photoenergy, 1-5.

Christensen, H., Sehested, K., Corfitzen, H., 1982. Reactions of hydroxyl radicals with hydrogen peroxide at ambient and elevated temperatures. J. Phys. Chem. 86, 1588-1590.

Criquet, J., Leitner, N.K.V., 2009. Degradation of acetic acid with sulfate radical generated by persulfate ions photolysis. Chemosphere 77, 194-200.

Daneshvar, N., Behnajady, M.A., Mohammadi, M.K.A., Dorraji, M.S.S., 2008. UV/H_2O_2 treatment of Rhodamine B in aqueous solution: Influence of operational parameters and kinetic modeling. Desalination 230, 16-26.

Dong, W.Y., Lee, C.W., Lu, X.C., Sun, Y.J., Hua, W.M., Zhuang, G.S., Zhang, S.C., Chen, J.M., Hou, H.Q., Zhao, D.Y., 2010. Synchronous role of coupled adsorption and photocatalytic oxidation on ordered mesoporous anatase TiO_2-SiO_2 nanocomposites generating excellent degradation activity of RhB dye. Appl. Catal. B Environ. 95, 197-207.

Fang, G.-D., Dionysiou, D.D., Wang, Y., Al-Abed, S.R., Zhou, D.-M., 2012. Sulfate radical-based degradation of polychlorinated biphenyls: Effects of chloride ion and reaction kinetics. J. Hazard Mater. 227, 394-401.

Getoff, N., F. Schworer, V.M. Markovic, K. Sehested, Nielsen, S.O., 1971. Pulse radiolysis of oxalic acid and oxalates. J. Phys. Chem. 75, 749-755.

GilPavas, E., Dobrosz-Gomez, I., Gomez-Garcia, M.-A., 2019. Optimization and toxicity assessment of a combined electrocoagulation, H_2O_2/Fe^{2+}/UV and activated carbon adsorption for textile wastewater treatment. Sci. Total Environ. 651, 551-560.

Grebel, J.E., Pignatello, J.J., Mitch, W.A., 2010. Effect of Halide Ions and Carbonates on Organic Contaminant Degradation by Hydroxyl Radical-Based Advanced Oxidation Processes in Saline Waters. Environ. Sci. Technol. 44, 6822-6828.

Grgic, I., Podkrajsek, B., Barzaghi, P., Herrmann, H., 2007. Scavenging of SO_4^- radical anions by mono- and dicarboxylic acids in the Mn(II)-catalyzed S(IV) oxidation in aqueous solution. Atmos. Environ. 41, 9187-9194.

Guan, Y.-H., Ma, J., Li, X.-C., Fang, J.-Y., Chen, L.-W., 2011. Influence of pH on the Formation of Sulfate and Hydroxyl Radicals in the UV/Peroxymonosulfate System. Environ. Sci. Technol. 45, 9308-9314.

He, Z., Sun, C., Yang, S., Ding, Y., He, H., Wang, Z., 2009. Photocatalytic degradation of rhodamine B by Bi2WO6 with electron accepting agent under microwave irradiation: Mechanism and pathway. J. Hazard Mater. 162, 1477-1486.

Hu, L., Deng, G., Lu, W., Lu, Y., Zhang, Y., 2017. Peroxymonosulfate activation by Mn_3O_4/metal-organic framework for degradation of refractory aqueous organic pollutant rhodamine B. Chinese Journal of Catalysis 38, 1360-1372.

Huang, Y., Wang, Z., Liu, Q., Wang, X., Yuan, Z., Liu, J., 2017. Effects of chloride on PMS-based pollutant degradation: A substantial discrepancy between dyes and their common decomposition intermediate (phthalic acid). Chemosphere 187, 338-346.

Isari, A.A., Payan, A., Fattahi, M., Jorfi, S., Kakavandi, B., 2018. Photocatalytic degradation of rhodamine B and real textile wastewater using Fe-doped TiO_2 anchored on reduced graphene oxide (Fe-TiO_2/rGO): Characterization and feasibility, mechanism and pathway studies. Appl. Surf. Sci. 462, 549-564.

Jiang, L., Zhang, Y., Zhou, M., Liang, L., Li, K., 2018. Oxidation of Rhodamine B by persulfate activated with porous carbon aerogel through a non-radical mechanism. J. Hazard Mater. 358, 53-61.

Keen, O.S., Linden, K.G., 2013. Degradation of Antibiotic Activity during UV/H_2O_2 Advanced Oxidation and Photolysis in Wastewater Effluent. Environ. Sci. Technol. 47, 13020-13030.

Khan, S., He, X., Khan, J.A., Khan, H.M., Boccelli, D.L., Dionysiou, D.D., 2017. Kinetics and mechanism of sulfate radical- and hydroxyl radical-induced degradation of highly chlorinated pesticide lindane in UV/peroxymonosulfate system. Chem. Eng. J. 318, 135-142.

Kim, M.H., Hwang, C.-H., Bin Kang, S., Kim, S., Park, S.W., Yun, Y.-S., Won, S.W., 2015. Removal of hydrolyzed Reactive Black 5 from aqueous solution using a polyethylenimine-polyvinyl chloride composite fiber. Chem. Eng. J. 280, 18-25.

Liang, C., Su, H.-W., 2009. Identification of Sulfate and Hydroxyl Radicals in Thermally Activated Persulfate. Ind. Eng. Chem. Res. 48, 5558-5562.

Liang, C.J., Lee, I.L., Hsu, I.Y., Liang, C.P., Lin, Y.L., 2008. Persulfate oxidation of trichloroethylene with and without iron activation in porous media. Chemosphere 70, 426-435.

Liu, X., Liu, Y., Lu, S., Wang, Z., Wang, Y., Zhang, G., Guo, X., Guo, W., Zhang, T., Xi, B., 2020. Degradation difference of ofloxacin and levofloxacin by UV/H_2O_2 and UV/PS (persulfate): Efficiency, factors and mechanism. Chem. Eng. J. 385.

Magazinovic, R.S., Nicholson, B.C., Mulcahy, D.E., Davey, D.E., 2004. Bromide levels in natural waters: its relationship to levels of both chloride and total dissolved solids and the implications for water treatment. Chemosphere 57, 329-335.

Masi, F., Rizzo, A., Bresciani, R., Martinuzzi, N., Wallace, S.D., Van Oirschot, D., Macor, F., Rossini, T., Fornaroli, R., Mezzanotte, V., 2019. Lessons learnt from a pilot study on residual dye removal by an aerated treatment wetland. Sci. Total Environ. 648, 144-152.

Nestmann, E.R., Douglas, G.R., Matula, T.I., Grant, C.E., Kowbel, D.J., 1979. Mutagenic activity of rhodamine dyes and their impurities as detected by mutation induction in Salmonella and DNA damage in Chinese hamster ovary cells. Cancer Res. 39, 4412-4417.

Neta, P., Huie, R.E., Ross, A.B., 1988. Rate constants for reactions of inorganic radicals in aqueous solution. J. Phys. Chem. Ref. Data 17, 1027-1284.

Nihemaiti, M., Miklos, D.B., Huebner, U., Linden, K.G., Drewes, J.E., Croue, J.-P., 2018. Removal of trace organic chemicals in wastewater effluent by UV/H_2O_2 and UV/PDS. Water Res. 145, 487-497.

Pouran, S.R., Aziz, A.R.A., Daud, W.M.A.W., 2015. Review on the main advances in photo-Fenton oxidation system for recalcitrant wastewaters. J. Ind. Eng. Chem. 21, 53-69.

Rao, Y., Han, F., Chen, Q., Wang, D., Xue, D., Wang, H., Pu, S., 2019. Efficient degradation of diclofenac by LaFeO3-Catalyzed peroxymonosulfate oxidation-kinetics and toxicity assessment. Chemosphere 218, 299-307.

Rao, Y.F., Xue, D., Pan, H.M., Feng, J.T., Li, Y.J., 2016. Degradation of ibuprofen by a synergistic UV/Fe(III)/Oxone process. Chem. Eng. J. 283, 65-75.

Rasheed, T., Bilal, M., Iqbal, H.M.N., Shah, S.Z.H., Hu, H., Zhang, X., Zhou, Y., 2018. TiO_2/UV-assisted rhodamine B degradation: putative pathway and identification of intermediates by UPLC/MS. Environmental Technology 39, 1533-1543.

Rehman, F., Sayed, M., Khan, J.A., Shah, N.S., Khan, H.M., Dionysiou, D.D., 2018. Oxidative removal of brilliant green by UV/$S_2O_8^{2-}$, UV/HSO_5^- and UV/H_2O_2 processes in aqueous media: A comparative study. J. Hazard Mater. 357, 506-514.

Semitsoglou-Tsiapou, S., Mous, A., Templeton, M.R., Graham, N.J.D., Leal, L.H., Kruithof, J.C., 2016. The role of natural organic matter in nitrite formation by LP-UV/H_2O_2 treatment of nitrate-rich water. Water Res. 106, 312-319.

Shankar, M.V., Nelieu, S., Kerhoas, L., Einhorn, J., 2007. Photo-induced degradation of diuron in aqueous solution by nitrites and nitrates: Kinetics and pathways. Chemosphere 66, 767-774.

Shen, Y.-S., Lin, C.-C., 2003. The effect of pH on the decomposition of hydrophenols in aqueous solutions by ultraviolet direct photolysis and the ultraviolet-hydrogen peroxide process. Water environment research : a research publication of the Water Environment Federation 75, 54-60.

Stefan, M.I., 2017. Advanced Oxidation Processes for Water Treatment: Fundamentals and Applications. IWA Publishing.

Su, S.N., Guo, W.L., Leng, Y.Q., Yi, C.L., Ma, Z.M., 2013. Heterogeneous activation of Oxone by $Co_xFe_{3-x}O_4$ nanocatalysts for degradation of rhodamine B. J. Hazard Mater. 244, 736-742.

Tian, F.-X., Ma, S.-X., Xu, B., Hu, X.-J., Xing, H.-B., Liu, J., Wang, J., Li, Y.-Y., Wang, B., Jiang, X., 2019. Photochemical degradation of iodate by UV/H_2O_2 process: Kinetics, parameters and enhanced formation of iodo-trihalomethanes during chloramination. Chemosphere 221, 292-300.

Wang, C., Hofmann, M., Safari, A., Viole, I., Andrews, S., Hofmann, R., 2019. Chlorine is preferred over bisulfite for H_2O_2 quenching following UV-AOP drinking water treatment. Water Res. 165.

Wang, F.G., Wang, W.J., Yuan, S.J., Wang, W., Hu, Z.H., 2017. Comparison of UV/H_2O_2 and UV/PS processes for the degradation of thiamphenicol in aqueous solution. J. Photoch. Photobio. A 348, 79-88.

Wang, P., Cheng, M., Zhang, Z., 2014. On different photodecomposition behaviors of rhodamine B on laponite and montmorillonite clay under visible light irradiation. Journal of Saudi Chemical Society 18, 308-316.

Wang, Y.R., Chu, W., 2011. Degradation of a xanthene dye by Fe(II)-mediated activation of Oxone process. J. Hazard Mater. 186, 1455-1461.

Westerhoff, P., Mezyk, S.P., Cooper, W.J., Minakata, D., 2007. Electron pulse radiolysis determination of hydroxyl radical rate constants with Suwannee river fulvic acid and other dissolved organic matter isolates. Environ. Sci. Technol. 41, 4640-4646.

Xu, X.-R., Li, X.-Z., 2010. Degradation of azo dye Orange G in aqueous solutions by persulfate with ferrous ion. Sep. Purif. Technol. 72, 105-111.

Zhang, T., Chen, Y., Wang, Y., Le Roux, J., Yang, Y., Croue, J.-P., 2014. Efficient Peroxydisulfate Activation Process Not Relying on Sulfate Radical Generation for Water Pollutant Degradation. Environ. Sci. Technol. 48, 5868-5875.

Zhang, T., Zhu, H., Croue, J.-P., 2013. Production of Sulfate Radical from Peroxymonosulfate Induced by a Magnetically Separable $CuFe_2O_4$ Spinel in Water: Efficiency, Stability, and Mechanism. Environ. Sci. Technol. 47, 2784-2791.

Zhang, Y., Luo, G., Wang, Q., Zhang, Y., Zhou, M., 2020. Kinetic study of the degradation of rhodamine B using a flow-through UV/electro-Fenton process with the presence of ethylenediaminetetraacetic acid. Chemosphere 240.

Zhang, Y., Xiao, Y., Zhong, Y., Lim, T.-T., 2019. Comparison of amoxicillin photodegradation in the UV/H_2O_2 and UV/persulfate systems: Reaction kinetics, degradation pathways, and antibacterial activity. Chem. Eng. J. 372, 420-428.

Zhao, X., Jiang, J., Pang, S., Guan, C., Li, J., Wang, Z., Ma, J., Luo, C., 2019. Degradation of iopamidol by three UV-based oxidation processes: Kinetics, pathways, and formation of iodinated disinfection byproducts. Chemosphere 221, 270-277.

Zhou, X., Zhou, Y., Liu, J., Song, S., Sun, J., Zhu, G., Gong, H., Wang, L., Wu, C., Li, M., 2019. Study on the pollution characteristics and emission factors of PCDD/Fs from disperse dye production in China. Chemosphere 228, 328-334.

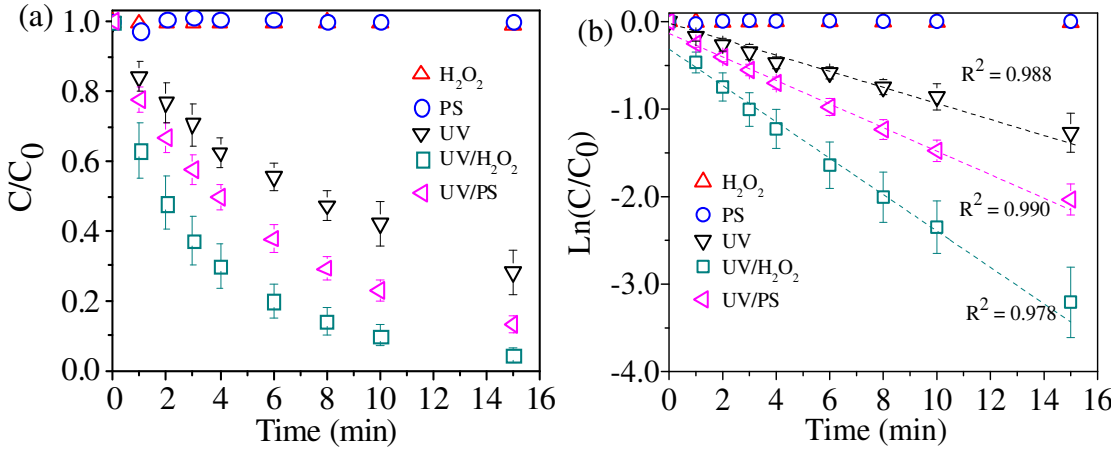

Fig. 1. (a) Relative degradation, and (b) pseudo-first-order kinetics of RhB in different oxidation systems. ($[RhB]_0$ = 10 μM, $[H_2O_2]_0$ = $[PS]_0$ = 50 μM, pH = 7)

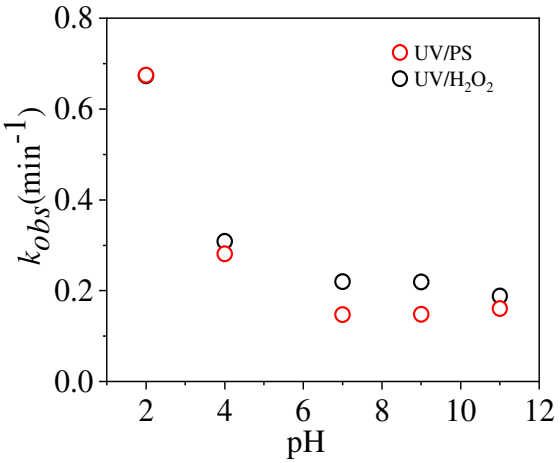

Fig. 2. Pseudo-first-order rate constant of RhB degradation under different initial solution pH in UV/H_2O_2 and UV/PS systems. ([RhB]$_0$ = 10 μM, [H_2O_2]$_0$ = [PS]$_0$ = 50 μM, pH = 7)

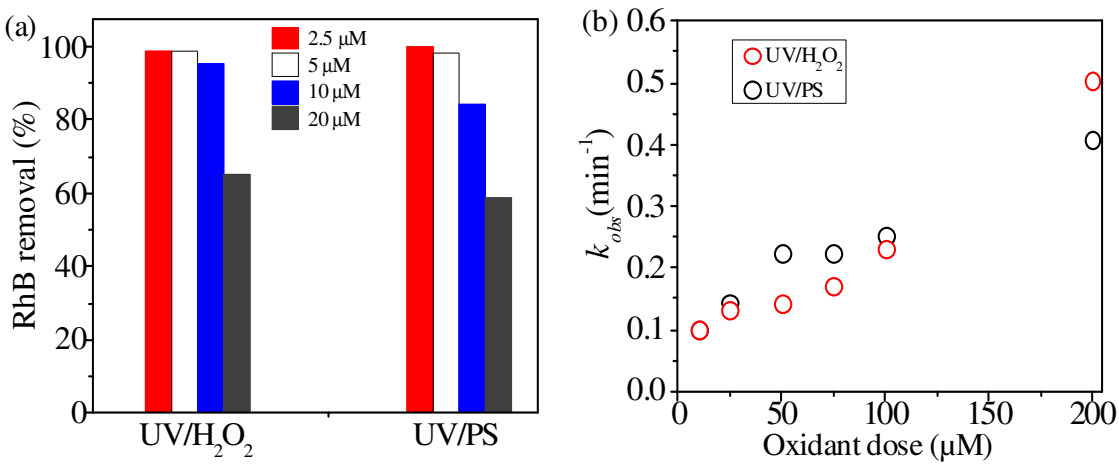

Fig. 3. RhB removal in UV/H_2O_2 and UV/PS systems under various (a) initial RhB concentration and (b) varying oxidant dose. ($[H_2O_2]_0 = [PS]_0 = 50$ μM, pH = 7)

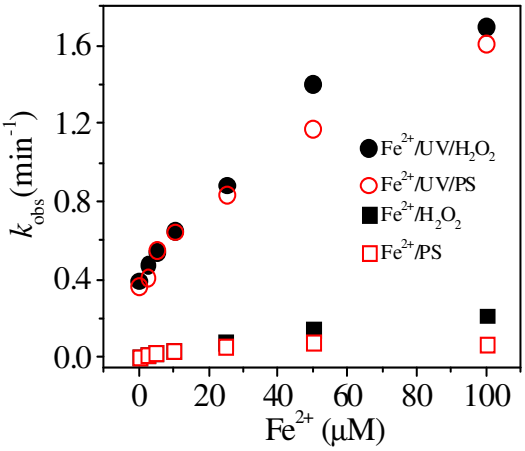

Fig. 4. Comparison of the pseudo-first-order rate constant (k_{obs}) of RhB degradation in different oxidation systems in the presence of Fe^{2+} as a transition metal activator. ($[RhB]_0$ = 10 μM, $[H_2O_2]_0$ = $[PS]_0$ = 50 μM, pH = 3)

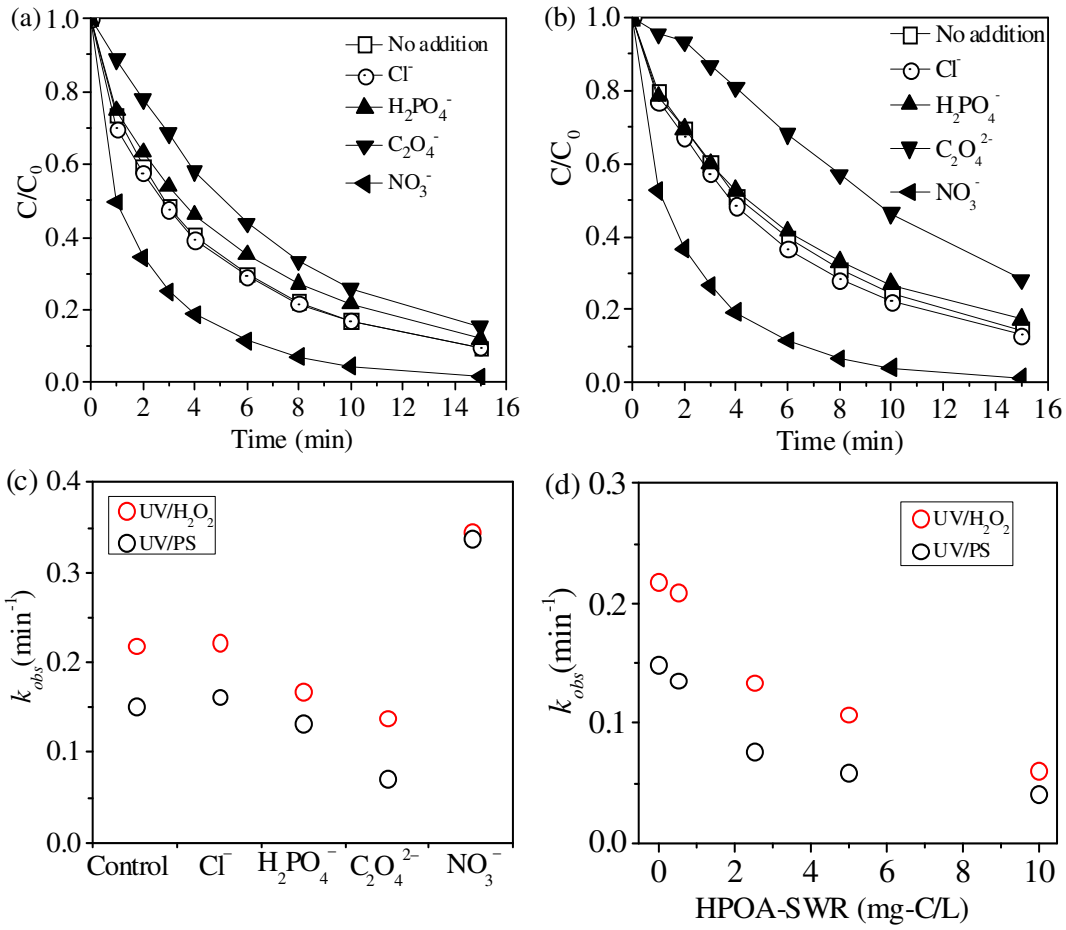

Fig. 5. Effect of different anions on the degradation of RhB in (a) UV/H_2O_2 and (b) UV/PS systems and the pseudo-first-order rate constants of RhB degradation in the presence of different anions (c) and varying concentrations of HPOA-SWR (d). ($[RhB]_0$ = 10 μM, $[H_2O_2]_0$ = $[PS]_0$ = 50 μM, $[Cl^-]_0$ = $[H_2PO_4^-]_0$ = $[C_2O_4^{2-}]_0$ = $[NO_3^-]_0$ = 10 mM, pH=7)

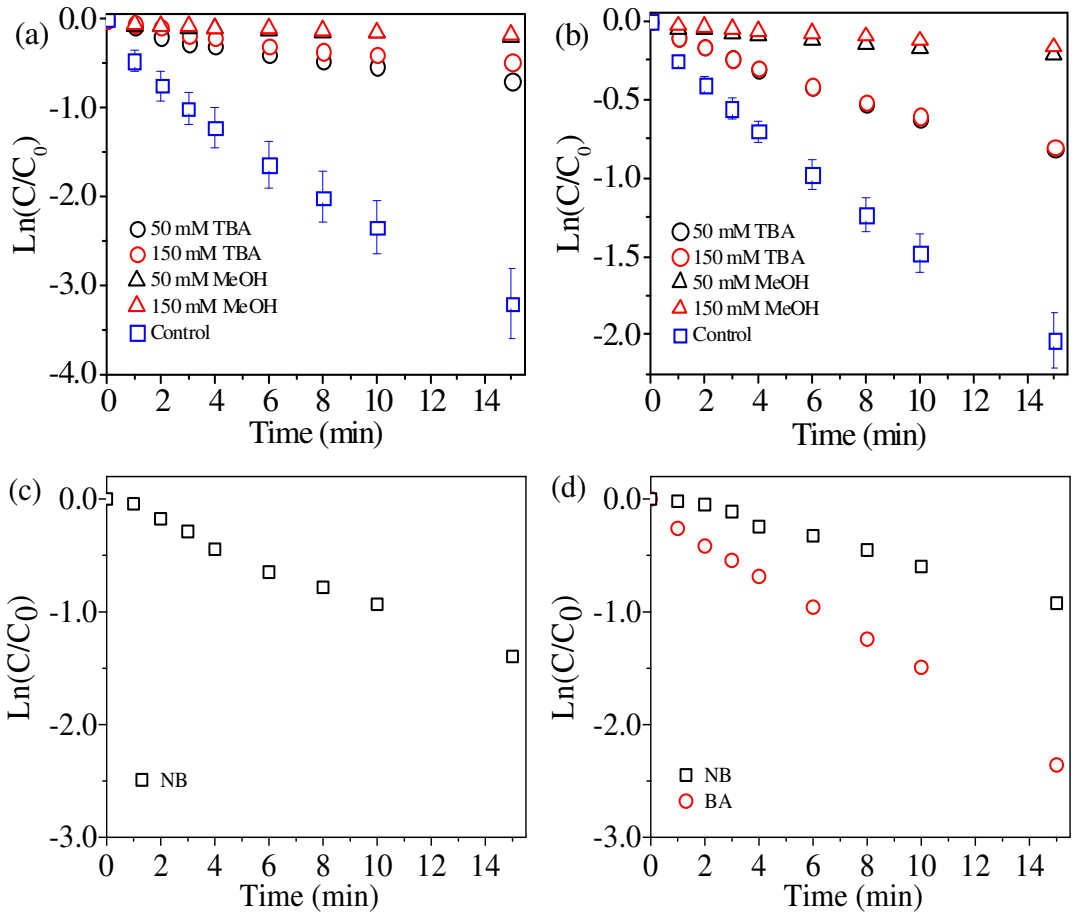

Fig. 6. The degradation of RhB in the presence of TBA or MeOH in (a) UV/H_2O_2 and (b) UV/PS systems, and the reaction kinetics of NB and BA degradation in the presence of 10 μM RhB in (c) UV/H_2O_2 and (d) UV/PS systems. ($[RhB]_0$ = 10 μM, $[H_2O_2]_0$ = $[PS]_0$ = 50 μM, $[NB]_0$ = $[BA]_0$ = 1 μM, pH = 7)

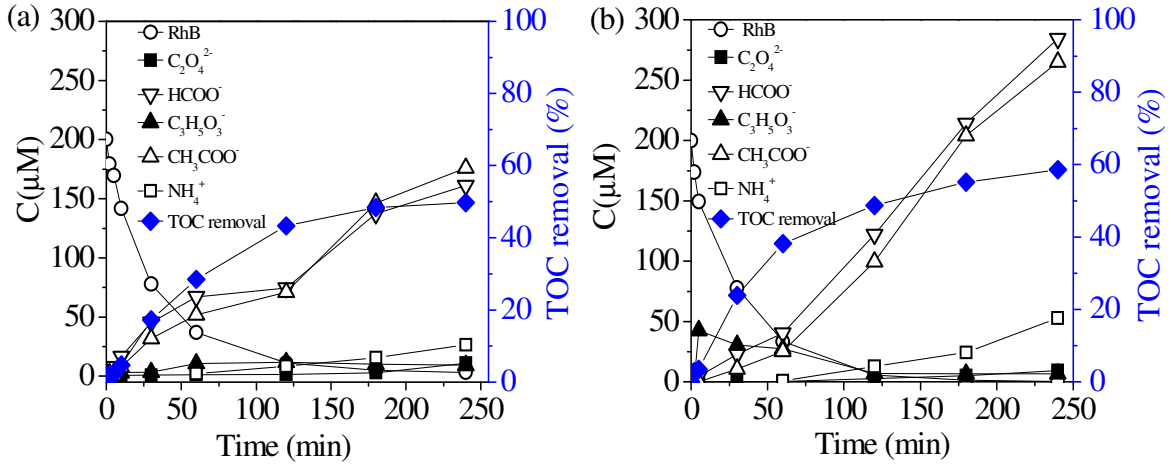

Fig. 7. Degradation and transformation of RhB and the subsequent formation of small molecular acids and NH_4^+ in (a) UV/H_2O_2 and (b) UV/PS systems. ($[RhB]_0$ = 0.2 mM, $[H_2O_2]_0$ = $[PS]_0$ = 1 mM, pH = 7)

Graphical Abstract